# Npas4 regulates medium spiny neuron physiology and gates cocaine-induced hyperlocomotion

Thomas Lissek[1,*] iD, Andry Andrianarivelo[2,3,4] iD, Estefani Saint-Jour[2,3,4], Marie-Charlotte Allichon[2,3,4], Hanke Gwendolyn Bauersachs[1], Merie Nassar[5], Charlotte Piette[5], Priit Pruunsild[1] iD, Yan-Wei Tan[1], Benoit Forget[2,3,4], Nicolas Heck[2,3,4], Jocelyne Caboche[2,3,4], Laurent Venance[5], Peter Vanhoutte[2,3,4,**] iD & Hilmar Bading[1,***] iD

## Abstract

We show here that the transcription factor Npas4 is an important regulator of medium spiny neuron spine density and electrophysiological parameters and that it determines the magnitude of cocaine-induced hyperlocomotion in mice. Npas4 is induced by synaptic stimuli that cause calcium influx, but not dopaminergic or PKA-stimulating input, in mouse medium spiny neurons and human iPSC-derived forebrain organoids. This induction is independent of ubiquitous kinase pathways such as PKA and MAPK cascades, and instead depends on calcineurin and nuclear calcium signalling. Npas4 controls a large regulon containing transcripts for synaptic molecules, such as NMDA receptors and VDCC subunits, and determines *in vivo* MSN spine density, firing rate, I/O gain function and paired-pulse facilitation. These functions at the molecular and cellular levels control the locomotor response to drugs of abuse, as Npas4 knockdown in the nucleus accumbens decreases hyperlocomotion in response to cocaine in male mice while leaving basal locomotor behaviour unchanged.

## Introduction

The central question in this study is what molecular components in striatal medium spiny neurons (MSNs) control information processing at the cellular level and the strength of hyperlocomotion upon cocaine administration in mice as a model for drug responsiveness in humans.

Drug addiction is a chronic and relapsing psychiatric disorder characterized by uncontrollable patterns of drug-seeking behaviour, leading to a loss of control over substance intake despite negative consequences. Experimental work has implicated behavioural responsiveness to a single drug dose in naïve rats as a predictor of individual addiction risk (Piazza *et al*, 1989). Deciphering the biological factors that regulate behavioural sensitivity to drugs of abuse is thus critical to better understand addiction susceptibility and will greatly aid in genetic drug abuse risk screening programmes as well as the development of potent prevention and treatment measures.

Striatal medium spiny neurons (MSNs) are crucial neuronal circuit elements for computing behavioural effects in response to drugs and in addiction. In line with their role as central CNS hubs, MSNs receive synaptic inputs from multiple brain regions (e.g. amygdala, prefrontal cortex, hippocampus and VTA) and integrate different neurotransmitter systems (i.e. dopamine and glutamate) to compute reward signals and direct behaviour accordingly (Britt *et al*, 2012; Kravitz *et al*, 2012). Hyperlocomotion upon cocaine treatment in naive animals depends on activity changes in D1-dopamine receptor (D1R)-expressing MSNs (Pierce & Kalivas, 1997; Hikida *et al*, 2010) and striatal D1 and NMDA receptors were shown to be necessary for full expression of the acute locomotion increase after cocaine administration (Pulvirenti *et al*, 1991; McGregor & Roberts, 1993) as well as for cocaine-dependent locomotor sensitization (Brown *et al*, 2011) (Kita *et al*, 1999). The tripartite synapse formed by glutamate and dopamine afferences converging onto the dendritic spines of MSNs is a privileged site of neurotransmitter integration where drug of abuse-evoked synaptic plasticity has been linked to behavioural alterations induced by cocaine (Pascoli *et al*, 2011b, 2014). At the morphological level, acute and repeated exposures to cocaine are able to alter MSN connectivity to glutamate and dopamine afferences (Heck *et al*, 2015; Dos Santos *et al*, 2017, 2018). MSN glutamatergic and dopaminergic inputs and the

structures associated with them (i.e. dendrites and spines) are hence crucial in mediating the behavioural effects of drugs of abuse and studying the molecular factors that regulate the activity of these entities will lead to a deeper understanding of the addiction process.

Interested in the molecular and cellular determinants of MSN function and their role in hyperlocomotion upon cocaine treatment, we chose to investigate the neuronal transcription factor Npas4 in detail. Npas4 is a basic helix-loop-helix transcription factor that is strongly expressed in the brain and induced by neuronal activity (Hester *et al*, 2007). In neurons, Npas4 was shown to be important for excitatory and inhibitory synaptogenesis and implied as a regulator of overall neuronal network function (Spiegel *et al*, 2014). Most studies so far focused on the role of Npas4 in hippocampal learning (Sun & Lin, 2016), with interesting recent data implicating it broadly in striatal reward-learning and drug-related behaviour (Taniguchi *et al*, 2017). These studies however did not bridge the molecular, cellular and network levels and leave open how Npas4 exerts its effects on behaviour. We therefore set out to analyse the molecular up- and downstream dependencies of Npas4 in MSNs and studied how Npas4 changes MSN function to impact acute and chronic drug-related behaviour.

## Results

### Npas4 is expressed in the nucleus accumbens and upregulated by repeated cocaine exposure

We analysed Npas4 expression in the striatum in the ventral parts (nucleus accumbens; NAc) and dorsal parts (dorsal Striatum, dStr)

by immunohistochemistry at different time points after five injections of cocaine in the home cage, which mimics a locomotor sensitization protocol, or saline control (Fig 1A). We found sparsely dispersed Npas4-positive neurons (i.e. NeuN-positive cells) at all time points in the saline group (Fig 1B and C), indicating that spontaneous activity or activity associated with the saline injection are enough to induce Npas4 in a small subset of cells. When compared to saline-treated mice, Npas4 expression was strongly upregulated in striatal neurons of the NAc 1 h after the last cocaine injection, but not at 30 min or 24 h. This transient induction of Npas4 was specific to the NAc since no significant difference was observed at any time point between the two groups in dStr (Fig 1C). In contrast, Fos was induced in both the NAc and dStr in the same animals (Fig EV1A and B) 1 h after cocaine administration, suggesting a more restricted induction mechanism of Npas4 that keeps its upregulation limited to the NAc.

### Npas4 induction is restricted to distinct synaptic stimuli

To dissect the molecular pathways involved in this more restricted Npas4 induction, we employed dissociated striatal neuron cultures from neonatal mice. These cultures contain mainly DARPP-32-positive MSNs (68% ± 3%, mean ± SEM; Fig 2A and B) and show robust and D1R-specific gene inductions upon treatment with the D1-agonist SKF-38393 (SKF) (Fig 2C). To investigate the main neurotransmitter input systems onto MSNs, we compared two models for synaptic stimulation—membrane depolarization via potassium chloride (HiK, 55 mM) (mimicking $Ca^{2+}$ influx after excitatory stimulation) and D1-receptor stimulation via SKF (10 μM)—for their ability to induce Npas4 transcription. Although both treatments induced the IEGs Arc, Egr1 and Inhba with similar
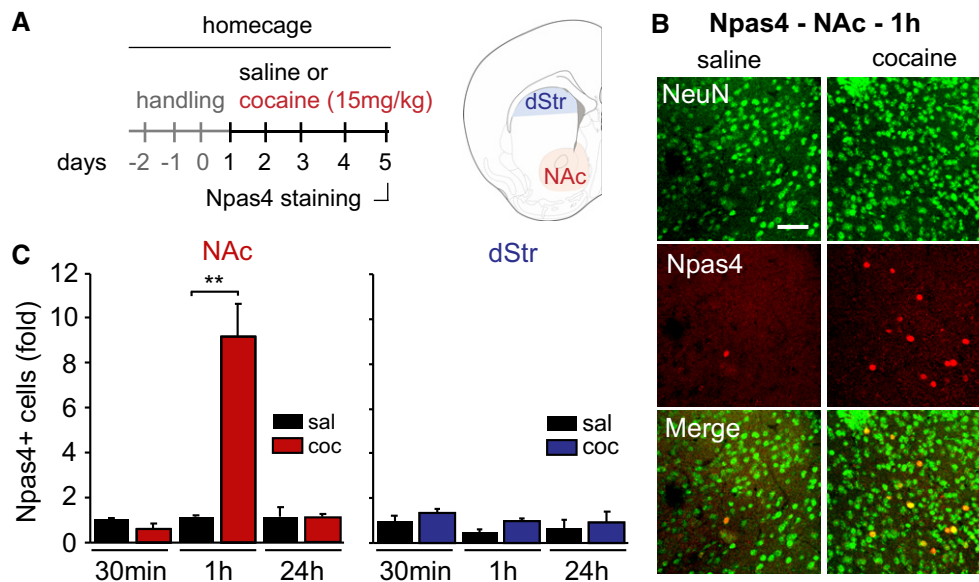


**Figure 1. Npas4 is sparsely expressed in the nucleus accumbens of saline-injected control animals and is upregulated by cocaine injection.**

A   Left: Time course of habituation and treatments with cocaine (15 mg/kg) or saline solutions. Right: striatal subdivisions where Npas4 expression was analysed by immunohistochemistry (NAc: nucleus accumbens; dStr: dorsal striatum).

B   Representative confocal images of NeuN (green) and Npas4 (red) immunostaining performed 1 h after the last injection of cocaine or saline (scale bar: 50 μm).

C   Quantifications of Npas4-positive cells (fold change normalized to the 30 min saline control group) in the NAc and dStr. Mean + SEM; *n* = 4 mice per group. 10 images (5 per hemisphere) per mouse for the NAc and 10 images (5 per hemisphere) for the dStr. **$P$ < 0.01, unpaired Student's *t*-test.
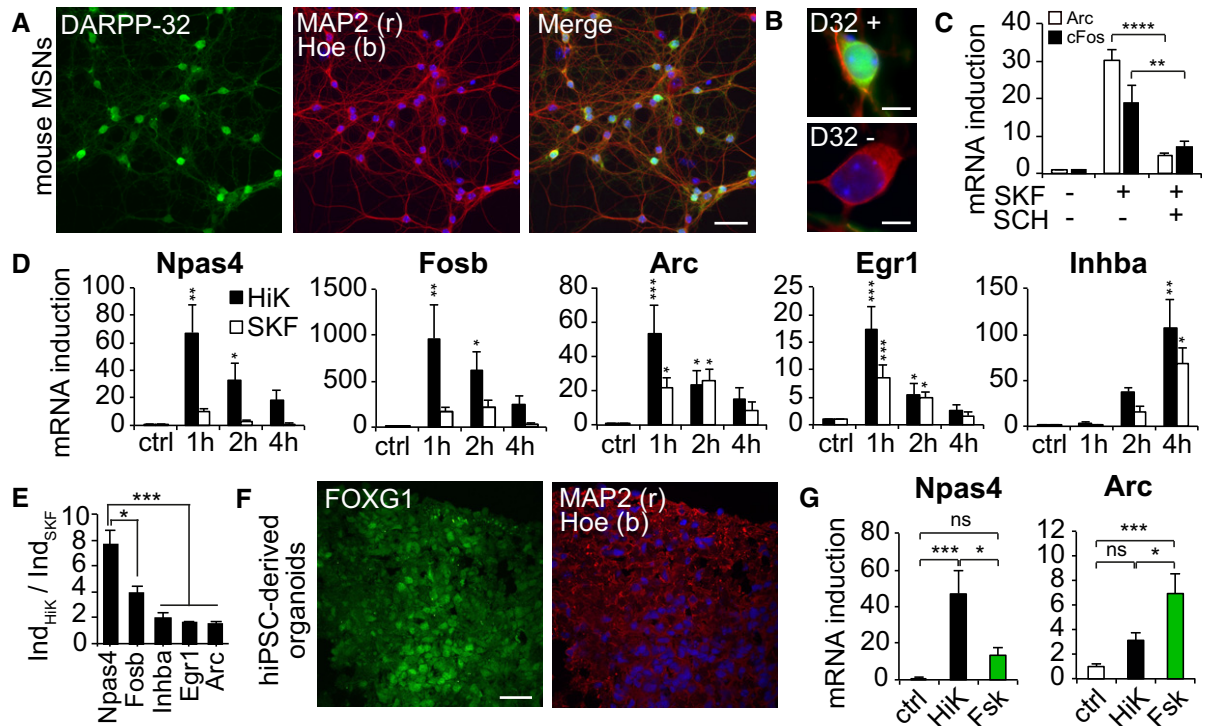
**Figure 2. Differential induction of Npas4 in mouse cultured medium spiny neurons and human iPSC-derived organoids through distinct stimuli.**

A  DARPP-32 (D32) immunostaining shows that striatal neuron cultures consist mainly of D32-positive medium spiny neurons (MSNs). 40× magnification, scale bar = 50 μm. MAP2 marks neurons, Hoechst (Hoe) stains DNA. *n* = 3 cultures from independent mouse litters.

B  100× magnification images show intracellular distribution of D32 in D32-positive neurons (D32 +). D32-negative neuron (D32 -) are shown for comparison. Scale bar = 10 μm.

C  MSN cultures at DIV11 were treated for 2 h with either 10 μM of the D1-agonist SKF-38393 (SKF) alone or with SKF and 10 μM of the selective D1-antagonist SCH-23390 (SCH). qPCR was performed to determine the relative mRNA levels of the immediate early genes cFos and Arc. Mean + SEM; one-way ANOVA with Holm-Sidak *post-hoc* correction; **$P < 0.01$, ****$P < 0.0001$; *n* = 3 independent cultures as biological replicates.

D  MSNs were depolarized with potassium chloride (HiK, 55 mM) or treated with the D1-agonist SKF-38393 (10 μM) for 1, 2 or 4 h. Subsequently, qPCR was performed to assess immediate early gene mRNA levels. Mean + SEM; two-way ANOVA with Bonferroni *post-hoc* test; indicated *P*-values for induction over control for each treatment; *$P < 0.05$, **$P < 0.01$, ***$P < 0.001$; *n* = 4 independent cultures as biological replicates.

E  To assess differences in mRNA load induced by HiK vs SKF, the values from the experiments in panel (D) were summed up over time for each treatment and the sums for each treatment were divided by each other to yield the ratio $I_{HiK}/I_{SKF}$. Values for this ratio were compared through one-way ANOVA with Tukey's *post-hoc* test; mean + SEM; *$P < 0.05$, ***$P < 0.001$; *n* = 4 independent cultures as biological replicates.

F  Immunohistochemistry analysis shows that cells in human iPSC-derived forebrain organoids express the forebrain neuron marker FOXG1 (green) and the neuron differentiation marker MAP2 (red). Hoe = Hoechst. Scale bar = 30 μm.

G  Differential induction of Npas4 through HiK and not forskolin in hiPSC-derived forebrain organoids. Organoids were treated with HiK (55 mM) or the PKA activator forskolin plus TTX (Fsk, 10 μM; TTX, 1 μM) for 1 h before qPCR analysis was performed to assess mRNA levels of Npas4 and Arc. Mean + SEM; *n* = 7 organoids in control condition, *n* = 5 organoids for HiK, *n* = 5 organoids for Fsk/TTX. One-way ANOVA with Tukey's *post-hoc* test, ns = not significant, *$P < 0.05$, ***$P < 0.001$.

magnitude, only membrane depolarization was able to robustly and significantly induce Npas4 (Fig 2D), with Fosb falling in the middle of these two groups. To correct for differences in temporal dynamics between the two stimuli and estimate total transcript load, we summed up the induction values over all time points for each treatment and divided them by one another ($Ind_{HiK}/Ind_{SKF}$), which revealed that Npas4 has a significantly higher value than all other IEGs analysed (Fig 2E), reflecting a primacy of membrane depolarization over D1R stimulation to induce Npas4. To assess the relevance of this phenomenon in humans, we analysed by qPCR in human iPSC-derived forebrain organoids whether differential inducibility of Npas4 is conserved in human neurons. Cells in these organoids express markers of differentiated neurons and forebrain neurons, MAP2 and FOXG1, respectively (Fig 2F). In line with our

findings in mouse neurons, Npas4 induction is higher after HiK stimulation than after a PKA-mediated transcriptional response triggered by forskolin/TTX (Fsk, 10 μM; TTX, 1 μM), while Arc is more strongly induced by Fsk/TTX than by HiK (Fig 2G).

**Npas4 induction depends on NMDA receptors, voltage-dependent calcium channels, nuclear calcium, CaMKII/IV and calcineurin, but is independent of PKA and MAPK signalling**

To dissect the signalling pathways involved in differential Npas4 induction, we stimulated mouse MSNs with HiK and co-applied pharmacological compounds to block ion channels or enzymes. The NMDA receptor blocker APV (100 μM) reduced all tested IEG inductions significantly after HiK (Fig 3A). This NMDA receptor

dependency of HiK-mediated gene inductions has been described previously and is due to the fact that NMDA receptors are activated by ambient glutamate in the culture medium (Macias *et al*, 2001; Pascoli *et al*, 2011a). Blockade of voltage-dependent sodium channels via TTX (1 μM) had no effect on gene inductions (Fig 3B). Further addition of the voltage-dependent calcium channel blocker verapamil (30 μM) to TTX reduced Npas4 and Fosb inductions significantly (Fig 3B). These results establish activity-dependent $Ca^{2+}$ channels as key regulators of Npas4 mRNA induction in MSNs. We next analysed the downstream kinases required for Npas4 upregulation. Traditionally, the main focus of synapse-to-nucleus communication in MSNs has been on the MAPK and PKA pathways. In the presence of the ERK1/2 inhibitor UO126 (10 μM) or the p38 blockers SB203580 (10 μM) and SB202190 (10 μM), induction of Arc and Fosb was significantly reduced (Fig 3C and D).

Surprisingly, none of the MAPK-inhibitors had an effect on Npas4 mRNA induction, indicating an independence of Npas4 induction from the MAPK pathway. The PKA inhibitor H-89 (10 μM) caused a significant blockade of Arc and left Fosb mRNA induction largely unaffected (Fig 3E). Interestingly, Npas4 was superinduced under H-89 treatment, which suggests that PKA might be a negative regulator of Npas4 induction while being a positive regulator of Arc induction. Co-incubation with the calcineurin blockers Cyclosporin A (1 μM) and FK506 (1 μM) attenuated Npas4 upregulation but had no effect on Arc and Fosb levels (Fig 3F). Blockade of CaMKII/IV activity via KN-93 (1 μM) resulted in a significant reduction in all assessed gene inductions (Fig 3G). To explore the possibility of crosstalk between $Ca^{2+}$ and D1-related signalling cascades, we co-applied HiK and SKF. Whereas co-stimulation with HiK and SKF lead to a super induction for Fosb, it had no significant effect on Arc
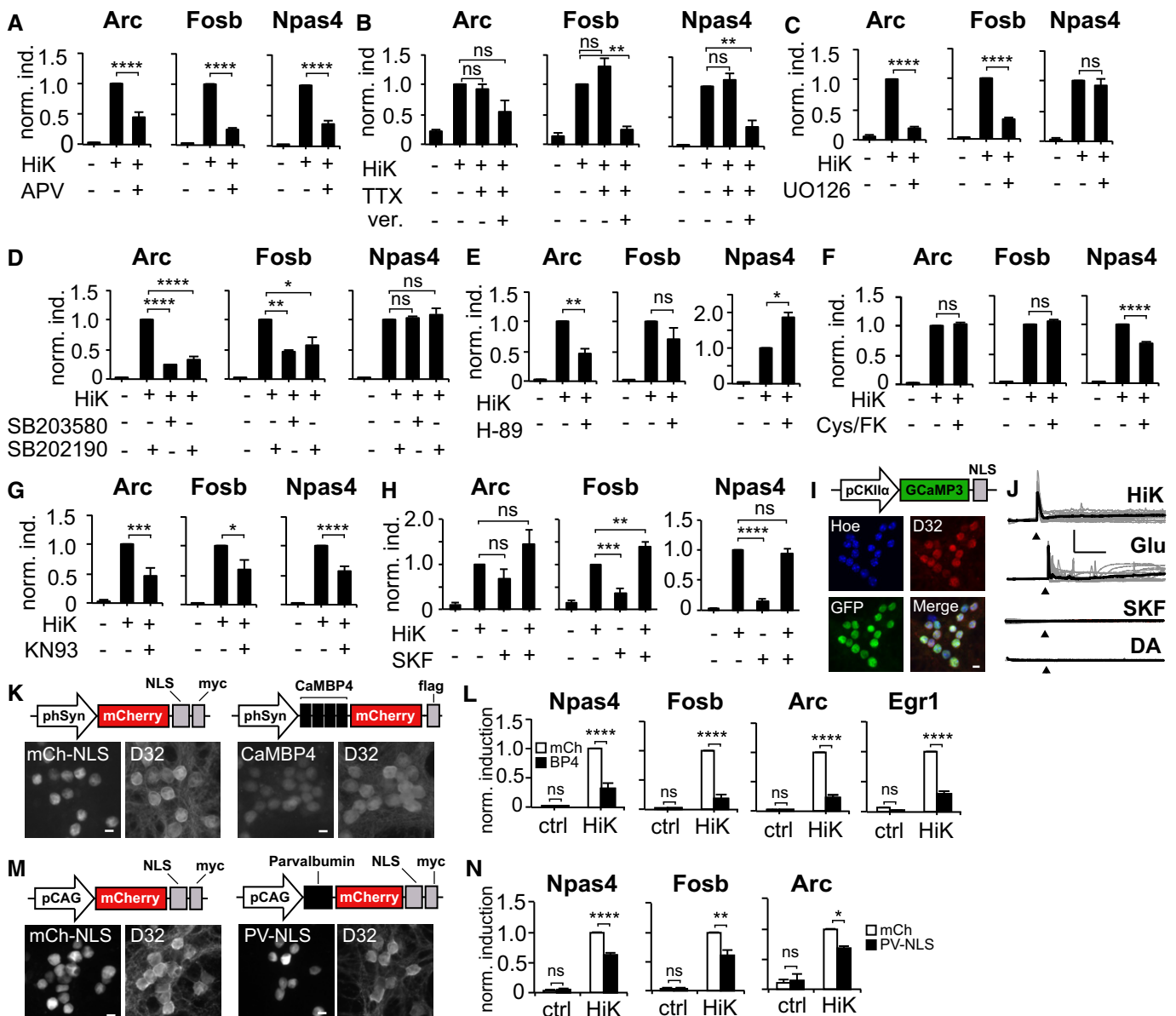


Figure 3.

◀

**Figure 3.   Npas4 induction depends on NMDA receptors, voltage-dependent calcium channels, CaMKII/IV, calcineurin and nuclear calcium and is independent of PKA and MAPK signalling.**

A–G  MSN cultures were stimulated with HiK (55 mM) for 1 h in the presence of various pharmacologicals to dissect the synapse-to-nucleus cascades mediating transcription of Npas4, Fosb and Arc. Values were normalized to the induced condition to compare for differences in induction between treatments. Mean + SEM and one-way ANOVA with Bonferroni *post-hoc* correction were used in all experiments. *$P < 0.05$, **$P < 0.01$, ***$P < 0.001$, ****$P < 0.0001$. *n*-number indicated in each panel. (A) Co-incubation with the NMDA receptor blocker APV (100 μM, applied 5 min before) reveals that all IEG inductions through HiK in MSNs depend on NDMA receptor activity. Mean + SEM; $n = 4$ independent cultures as biological replicates. (B) Blockade of voltage-dependent calcium channels through verapamil (30 μM, 5 min before) and TTX (1 μM, 5 min, to prevent verapamil-induced bursting) leads to significant reduction in gene inductions for Npas4 and Fosb. Mean + SEM; $n = 4$ independent cultures as biological replicates. (C) Inhibition of ERK1/2 through UO126 (10 μM, 20 min before) leads to significant blockade of mRNA induction for Arc and Fosb, but not Npas4. Mean + SEM; $n = 3$ independent cultures as biological replicates. (D) Inhibition of p38alpha and p38beta through SB203580 or SB202190, respectively (both 10 μM and 20 min before) leads to significant reductions in mRNA induction for Arc and Fosb, but not Npas4. Mean + SEM; $n = 3$ independent cultures as biological replicates. (E) Blockade of PKA activity through H-89 (10 μM, 20 min before) leads to reduced induction of Arc, unaffected induction of Fosb and a superinduction of Npas4. Mean + SEM; $n = 3$ independent cultures as biological replicates. (F) Inhibition of calcineurin through co-application of Cyclosporin and FK506 (1 μM each, 20 min before) leads to unaffected induction of mRNAs for Arc and Fosb, but significantly reduced levels of Npas4. Mean + SEM; $n = 3$ independent cultures as biological replicates. (G) Blockade of CaMKII/IV through application of KN-93 (1 μM, 20 min before) leads to significantly reduced mRNA inductions of Arc, Fosb and Npas4. Mean + SEM; $n = 4$ independent cultures as biological replicates.

H  Co-application of HiK and SKF reveals synergistic effects on mRNA induction of Fosb but not Arc or Npas4, Mean + SEM; $n = 6$ independent cultures as biological replicates.

I–N  Investigating the role of nuclear calcium signalling in mRNA induction of Arc, Fosb and Npas4. (I) Immunohistochemical analysis of MSNs infected with rAAV-pCKIIa-GCaMP3-NLS. Infection on DIV5, fixation on DIV12. Hoe = Hoechst, D32 = anti-Darpp-32, GFP = anti-GFP, 40× magnification, scale bar = 10 μm. (J) Nuclear calcium imaging of MSN cultures after application of different stimuli. HiK (55 mM), glutamate (Glu, 1 μM), SKF-38393 (SKF, 10 μM) or dopamine (DA, 20 μM) were applied after ~10 min of baseline imaging (arrowheads). Grey traces indicate individual cells, black traces indicate mean of all imaged cells (~30) for one stimulation run. inset: *y*-axis: 100% Δ*F/F*, *x*-axis: 10 min, $n = 3$ independent cultures. (K) immunohistochemical analysis of MSNs infected with mCherry-NLS as control or the competitive nuclear Ca$^{2+}$/CaM antagonist CaMBP4-mCherry. Infection on DIV4, fixation on DIV11. D32 = anti-Darpp-32. scale bar = 10 μm. (L) MSNs expressing rAAV-mCherry-control or CaMBP4 (BP4) were treated with 55mM HiK for 1 h and qPCR analysis was performed for the indicated IEGs. Mean + SEM; two-way ANOVA with Bonferroni *post-hoc* test, ns = not significant, ****$P < 0.0001$. $n = 5$ independent cultures as biological replicates. (M) Immunohistochemical analysis of MSNs infected with mCherry-NLS as control or the nuclear Ca$^{2+}$-buffer Parvalbumin-NLS-mCherry. Infection on DIV4, fixation on DIV11. D32 = anti-Darpp-32. (N) MSNs expressing rAAV-mCherry-control or PV-NLS were treated with 55mM HiK for 1 h and qPCR analysis was performed for the indicated IEGs. Mean + SEM; two-way ANOVA with Bonferroni *post-hoc* test, *$P < 0.05$, **$P < 0.01$, ****$P < 0.0001$. $n = 3$ independent cultures as biological replicates.

or Npas4 (Fig 3H). Together, the above results indicate that at least two sets of IEGs exist in MSNs: (i) classical IEGs (i.e. Arc) that are regulated by well-studied signalling cascades such as the MAPK and PKA pathways and thus induced by both depolarization and D1-receptor activation, and (ii) genes that are selectively induced after membrane depolarization (i.e. Npas4) and independent of MAPK and PKA pathways but dependent on CaN and CaMKII/IV. While CaN and CaMKII/IV are shown to be regulators downstream of Ca$^{2+}$ influx, this experimental set leaves open the question of which synapse-to-nucleus signal regulates Npas4 induction in MSNs. Previous studies in hippocampal neurons have identified Npas4 to be dependent on nuclear calcium signalling (Zhang *et al*, 2009). If Npas4 expression is indeed tightly controlled by nuclear calcium influx in MSNs, HiK and Glu should evoke nuclear calcium transients while SKF and DA should not. We tested this hypothesis by calcium imaging with the nuclear-localized Ca$^{2+}$ indicator GCaMP3-NLS (Fig 3I). Addition of HiK or Glu lead to robust increases in nuclear calcium while addition of SKF or DA proved to be ineffective (Fig 3J). To test for necessity of nuclear calcium signalling for Npas4 induction, we then infected cells with an rAAV encoding for CaMBP4, a nuclear localized peptide antagonist of Ca$^{2+}$/CaM signalling, and analysed gene inductions after HiK stimulation via qPCR. We found that inductions of all analysed genes including Npas4 were significantly blocked by CaMBP4 (Fig 3K and L), indicating that nuclear calcium is a necessary synapse-to-nucleus signal for IEG induction in MSNs after membrane depolarization. Because expression of CaMBP4 might lead to chronic adaptations that reduce IEG inducibility by non-acute means (i.e. through nuclear HDAC accumulation [Schlumm *et al*, 2013]), we infected cells with an rAAV encoding a nuclear localized version of the protein calcium buffer Parvalbumin (PV-NLS). While no effects on basal expression

were observed, PV-NLS significantly reduced induction of Npas4, Arc and Fosb after HiK stimulation (Fig 3M and N).

## Npas4 regulates a large transcript set, including mRNAs for glutamatergic synapse proteins and voltage-gated Ca$^{2+}$ channel subunits

We next asked what the downstream functions of differentially regulated Npas4 are and reasoned that restriction of Npas4 induction to distinct stimuli might tightly control a unique and potent transcriptional response. We performed transcriptome microarray analysis of hippocampal neurons after rAAV-mediated Npas4 over-expression and observed an at least 1.5-fold increase in the levels of 1,091 sequences and an at least 1.5-fold decrease in levels of 1,133 sequences compared to the GFP control (Fig 4A, Dataset EV1). To investigate what biological processes Npas4 regulates, we analysed the Npas4 regulon with the PANTHER classification system (Fig 4B, Datasets EV2 and EV3, see Materials and Methods for details) and gene ontology (GO) analysis for biological processes. Noteworthy, among others, were enrichments for the following biological processes: regulation of synapse assembly, regulation of synapse organization, regulation of synapse structure or activity, learning or memory, regulation of locomotion, behaviour, nervous system development, regulation of dendrite morphogenesis, cognition and regulation of synaptic plasticity. The above findings imply Npas4 to be a potential master regulator of neuronal physiology and behaviour with a large target gene programme, allowing for profound and long-lasting changes in neuronal function and structure. To complete the microarray analysis, we manually analysed the Npas4 regulon for entities that are commonly altered in addiction and reward-related processes and found various relevant genes, such as

those involved in glutamate signalling (i.e. Nptx2, Grin1, Gria2, Gria3, Homer2, Grm5), dopamine signalling (i.e. Darpp-32, Drd4, Rcs/Arpp-21) and dendrite morphogenesis (i.e. Vegfd/Figf) (Fig 4C) among many others. Interestingly, Npas4 seems to regulate important synaptic proteins (i.e. Nptx2) and $Ca^{2+}$ channel subunits (i.e. Grin1). To further analyse this phenomenon in MSNs, we
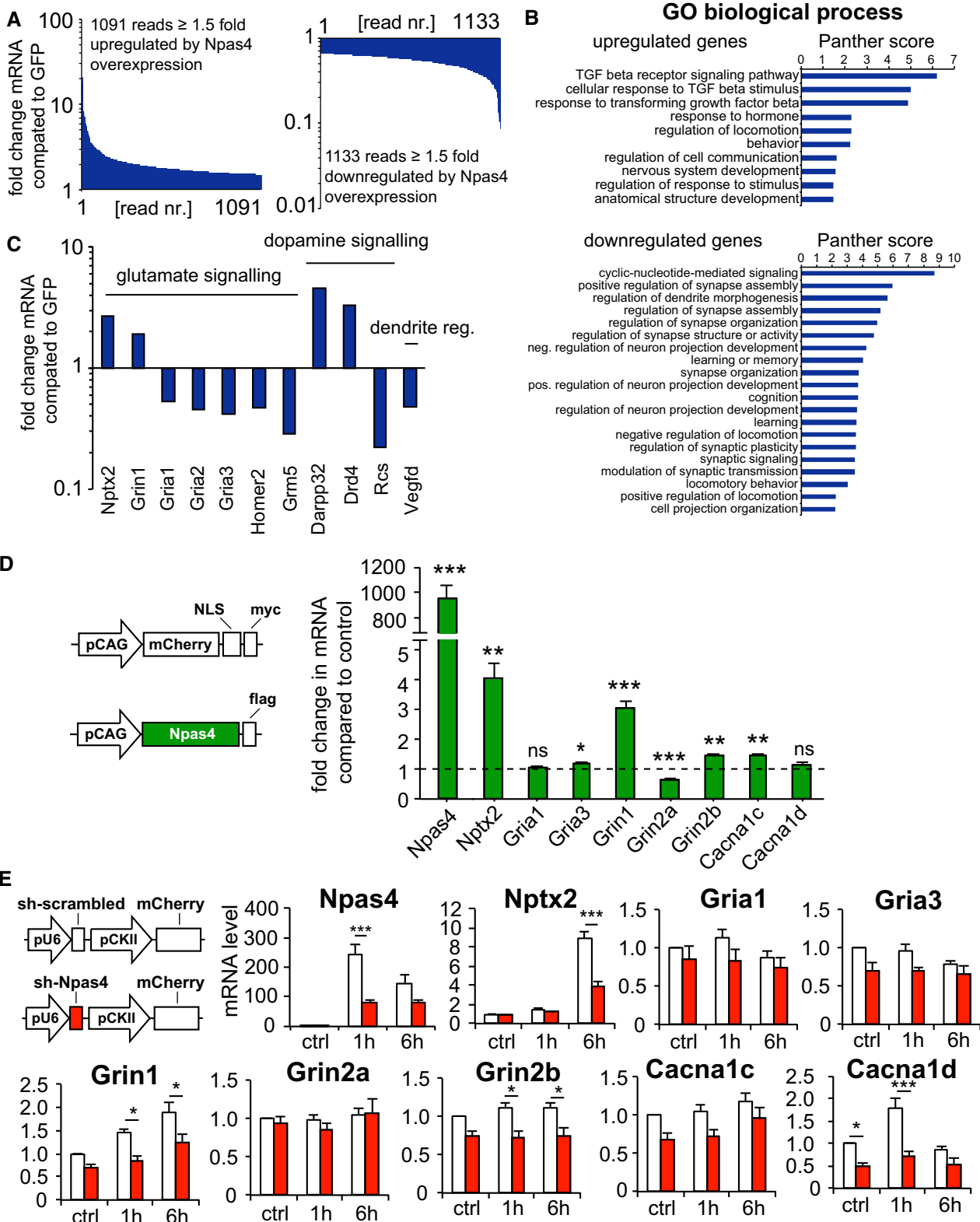


**Figure 4.**

◀

> **Figure 4.  Npas4 overexpression affects a large mRNA set including transcripts encoding NMDA receptors and subunits for Ca$^{2+}$ channels.**
>
> A–C  Hippocampal neurons were infected with rAAVs expressing GFP (control) or Npas4 (Npas4 overexpression) on DIV4. On DIV11, RNA was harvested and subjected to microarray transcript analysis. (A) Overexpression of Npas4 leads to ≥ 1.5-fold upregulation of the levels of 1,091 sequences and to a ≥ 1.5-fold downregulation of the levels of 1,133 sequences, indicating that Npas4 regulates a widespread transcriptional response. (B) gene ontology analysis (GO) for biological processes via the Panther tool for up- and downregulated genes from panel (A). Shown is a selection of relevant processes. Upregulated genes are enriched for cell-signalling processes (i.e. TGF-beta signalling, hormone responses), behaviour (i.e. locomotion) and developmental processes (i.e. anatomical structure development). Downregulated genes are enriched for synapse regulation (i.e. regulation of synapse assembly), dendritic organization (i.e. dendrite morphogenesis) and cognitive processes (i.e. learning, cognition, locomotion). (C), selection of genes from the Npas4 regulon with relevance to synaptic transmission and dendrite morphology, both of which are processes implicated in habitual learning.
> D  Npas4 overexpression leads to basal upregulation of genes encoding for proteins targeted to glutamatergic synapse function and Ca$^{2+}$ channels in MSNs. MSNs were infected with rAAVs expressing mCherry-NLS control or Npas4 on DIV4 or DIV5 and expression of the indicated genes was analysed by qPCR on DIV11 or DIV12. Shown are mRNA levels normalized to mCherry-control. The dashed line represents normalized control levels. pCAG = CAG promoter, myc = myc-tag, flag = flag-tag. Mean + SEM; unpaired, two-tailed *t*-test for each gene, \**P* < 0.05, \*\**P* < 0.01, \*\*\**P* < 0.001. *n* = 5 independent cultures as biological replicates.
> E  Npas4 controls activity-dependent upregulation of genes for glutamatergic synapse formation and Ca$^{2+}$ channels. MSNs were infected with rAAVs expressing shRNA-scrambled (control) or shNpas4 (Npas4 knockdown) on DIV5. On DIV 12, cultures were stimulated with HiK (55 mM) for 1 or 6 h and mRNA levels were analysed by qPCR. mRNA level = fold change in mRNA compared to shscrambled unstimulated control. Mean + SEM; two-way ANOVA with Bonferroni *post-hoc* test, \**P* < 0.05, \*\*\**P* < 0.001. *n* = 5 independent cultures as biological replicates.

overexpressed Npas4 via rAAV and performed a qPCR analysis for the synaptic protein-encoding transcripts Nptx2, Gria1, Gria3 and transcripts for the calcium channel subunits Grin1, Grin2a, Grin2b, Cacna1c and Cacna1d. We found significant upregulations for Nptx2, Gria3, Grin1, Grin2b and Cacna1c and a highly significant downregulation in Grin2a (Fig 4D). To complement the overexpression experiments and test whether these molecular changes are induced by Npas4 in an acute manner, we performed qPCR analysis after shRNA-mediated knockdown of Npas4 and HiK stimulation. We find that Npas4 knockdown significantly decreases activity-dependent transcript levels of Nptx2, Grin1, Grin2b and Cacna1d (Fig 4E).

**Npas4 regulates MSN spine density *in vivo***

In our *in vitro* transcriptome analysis, we found that Npas4 regulates gene sets implicated in synapse formation (Fig 4B, GO terms "regulation of synapse assembly", "regulation of synapse organization", "regulation of synapse structure or activity"; mRNA upregulation of Nptx2, Grin1 and Grin2b). To study the role of Npas4 in dendritic spine function, we performed rAAV-shRNA-mediated knockdown of Npas4 *in vivo* and analysed MSN spine density from mice that were subjected to repeated saline or cocaine injections (Fig 5A). To enable

3D analysis of D1R-MSN morphology, we sparsely labelled this cell type by co-injecting a mix of AAV-PPTA-Cre, which drives a D1R-MSN-specific expression of the Cre recombinase, and AAV-flex-tdTomato in a 1:10,000 ratio (Fig 5B). The morphological analysis was performed in the shell part of the NAc 1d after the last injection of cocaine or saline, in td-Tomato-positive (i.e. D1R-positive) MSNs infected with rAVV-sh-Npas4, which triggered a robust knockdown of Npas4 as compared to control (Fig 5C and D). The analysis of dendritic spine density (Fig 5E and F) revealed that Npas4 knockdown decreased D1R-MSN spine density under basal conditions in the saline-treated group and prevented the cocaine-evoked increase in dendritic spine density that was observed in the scrambled shRNA control group. Npas4 knockdown had no effect on spine head diameter in either the saline- or cocaine-treated animals (Fig EV2A). To complement the analysis in D1-MSNs, we performed the same set of experiments in D2R-MSNs. D2R-MSNs were labelled with the same Cre-AAV-mediated approach as for D1R-MSNs, except that cells were infected with AAV-ENK-Cre (Fig 5G) instead of AAV-PPTA-Cre. There were no significant differences in spine density in any treatment group in D2R-MSNs (Fig 5H) and no differences in spine head diameter (Fig EV2B), indicating that Npas4-mediated regulation of spine density is restricted to D1-MSNs.

> **Figure 5.  Npas4 regulates dendritic spine density in D1R-MSNs under basal conditions and after repeated cocaine exposure.**                                   ▶
>
> A  Time course of AAV injections, habituation and treatments to assess the impact of Npas4 knockdown on MSN neuronal morphology under basal conditions and after repeated cocaine injections.
> B  Representative images of AAV-shscr-GFP- and AAV-shNpas4-GFP-infected cells together with the sparse labelling of D1R-MSNs achieved through a co-injection of AAV-Flex-tdTomato and AAV-PPTA-Cre (to label D1 MSNs) or AAV-ENK-Cre (to label D2 MSNs) in a 1/10,000 ratio. Scale bar = 100 μm.
> C  Representative confocal images of staining for Npas4 expression (red) in the NAc of mice infected with AAV shscr-GFP or AAV-shNpas4-GFP 1 h after cocaine treatment. Scale bar = 20 μm. Note the presence of Npas4-positive neurons infected with the AAV shscr-GFP (arrowheads) and not in cells infected with the AAV-shNpas4.
> D  Quantifications of GFP-positive and Npas4-positive cells 1 h post cocaine treatment. Data were normalized so that the number of GFP- and Npas4-positive cells was set to 100%. 20 fields of view were analysed from *n* = 3 mice in the case of AAV-shscr-GFP and 30 fields of view from *n* = 3 mice for AAV-shNpas4-GFP. Mean + SEM; unpaired Student's *t*-test; \**P* < 0.05, *n* = 3 mice per group.
> E  Confocal images of tdTomato-labelled D1-MSNs expressing shscr-GFP or shNpas4-GFP (left panels; scale bar: 20 μm). 3D volume-renderings of MSN dendrites from the NAc shell (right panels; scale bar: 2 μm).
> F  Quantification of spine density in D1-MSNs, defined as the number of spines normalized to 10μm of dendrite for saline control and after cocaine injection. Mean + SEM; two-way ANOVA, Bonferroni *post-hoc* test, \**P* < 0.05; \*\**P* < 0.01; \*\*\**P* < 0.001. *n* = 40 neurons from 4 mice in each experimental group.
> G  Confocal images of tdTomato-labelled D2-MSNs expressing shscr-GFP or shNpas4-GFP (left panels; scale bar: 20 μm). 3D volume-renderings of MSN dendrites from the NAc shell (right panels; scale bar: 2 μm).
> H  Quantification of spine density in D2-MSNs, defined as the number of spines normalized to 10μm of dendrite for saline control and after cocaine injection. Mean + SEM; two-way ANOVA, Bonferroni *post-hoc* test, all non-significant. *n* = 40 neurons from 4 mice in each experimental group.
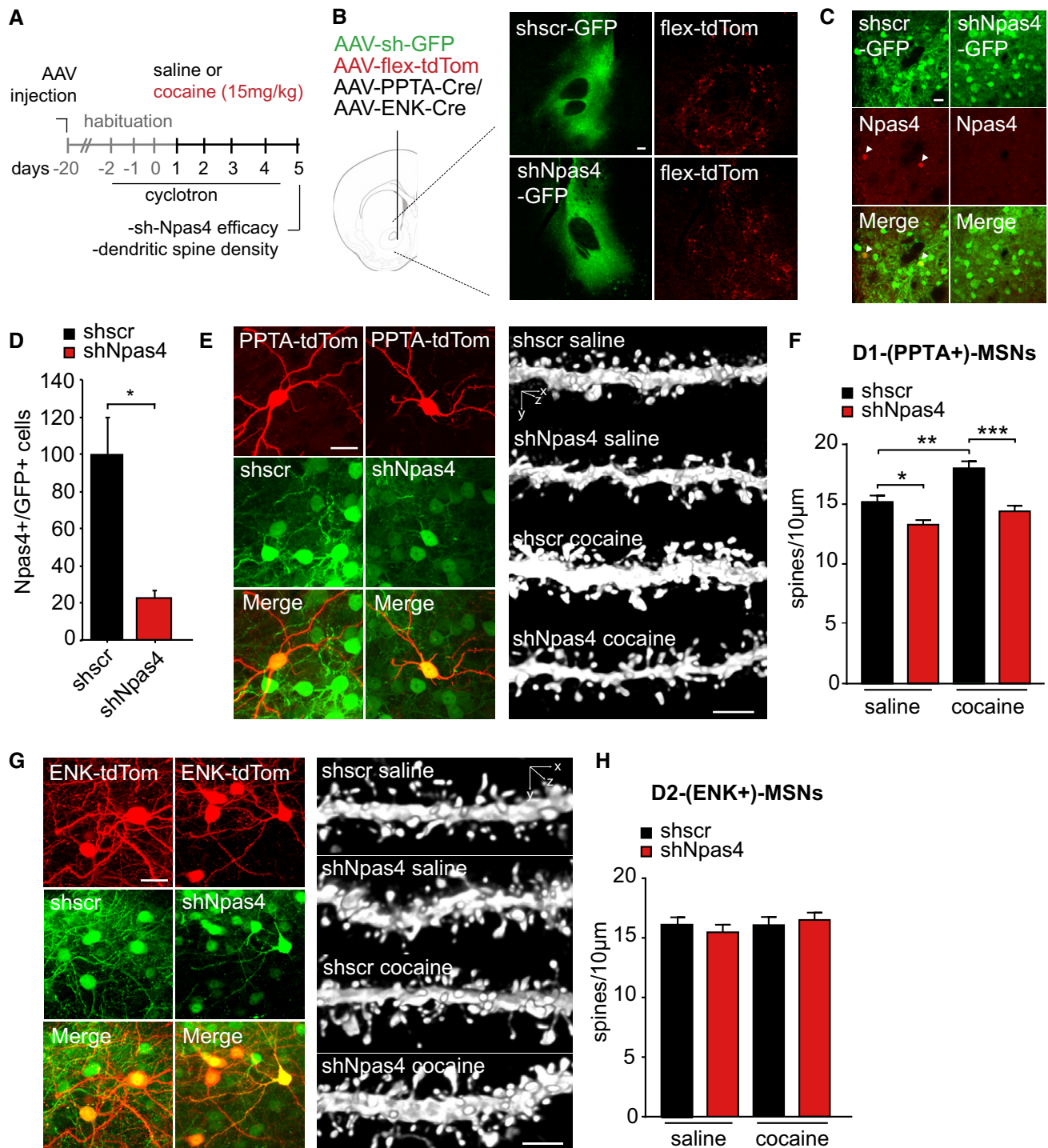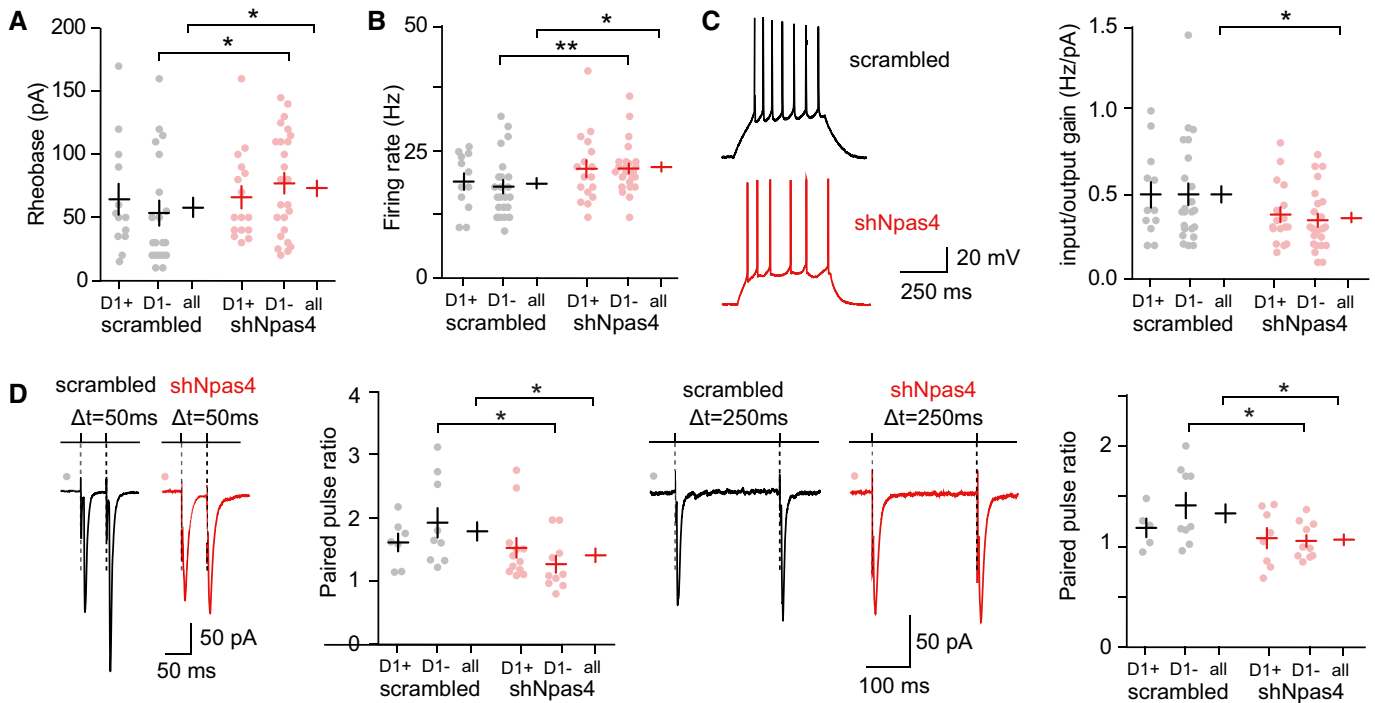
**Figure 5.**

## Npas4 controls MSN electrophysiological properties

To evaluate the impact of Npas4 on key synaptic and membrane properties in MSNs, we conducted an electrophysiological analysis of intrinsic cellular parameters and corticostriatal synaptic transmission in *ex vivo* slice preparations from adult mice injected with rAAV-shNpas4 (Fig 6). We have differentiated D1-positive and D1-negative MSNs through the $D_1$-tdTomato rAAV labelling approach used in the dendritic spine analysis and analysed these two neuron populations separately and pooled to study overall effects on MSN physiology. We examined 15 active and passive membrane properties (Table EV1) and found an increased rheobase (Fig 6A) and firing rate (Fig 6B) and a decreased input/output gain function (Fig 6C) in the Npas4-knockdown mice compared to control. The

**Figure 6. Npas4 regulates MSN membrane excitability and corticostriatal transmission.**

A–D Scatter plot of passive and active membrane properties of MSNs in *ex vivo* slice preparations from shRNA-AAV-infected mice, plotted for MSNs as D1-positive (D1+), D1-negative (D1-) and those two populations pooled (all). (A) rheobase; mean ± SEM. (B) Firing rate estimated at twice the value of the rheobase; mean ± SEM. (C) input/output gain values recorded in shscr- or shNpas4-injected mice, mean ± SEM. The increased rheobase and lower input-output gain indicate a lower excitability for MSNs in the Npas4-knockdown group. (D) facilitation at corticostriatal synapses examined in MSNs with paired-pulse stimulation at 20 and 4 Hz. Representative current traces and scatter plots of paired-pulse experiments illustrate a potent facilitation in MSNs in mice injected with scr-shRNA and a significant decrease of the facilitation in mice injected with shNpas4, with a stronger effect in D1-negative MSNs. Mean ± SEM.

Data information: For *n*-numbers, please see Table EV1. Mann–Whitney-Test, *P < 0.05, **P < 0.01.

rheobase and firing rate increases were primarily present in D1-negative MSNs and pooled cells, whereas the I/O gain decrease had similar effect sizes in D1-positive and D1-negative MSNs, although only the pooled cell group was statistically significant in this experimental set. Together, these findings indicate a lower MSN excitability in the AAV-shNpas4-injected mice. We observed no difference for membrane resting potential, input resistance or other AP features (Table EV1). We next recorded EPSCs evoked by paired-pulse stimulations at 20 and 4 Hz to assess the probability of release (Fig 6D). Paired-pulse ratio (PPR) analysis revealed that in control mice, the corticostriatal short-term plasticity was facilitated for 20 and 4 Hz paired-pulse stimulations (Fig 6D and Table EV1). In the shNpas4 injected mice, facilitation was still observed but was significantly decreased at both 20 and 4 Hz stimulations (Fig 6D). The observed effects were due to significant changes in D1-negative MSNs, whereas D1-positive MSNs did not show changes in short-term plasticity. This decreased facilitation indicates an increase in the probability of glutamate release from pyramidal cells.

**Npas4 regulates hyperlocomotion in response to the first cocaine injection and throughout the course of cocaine-induced sensitization**

In addition to its roles in MSN spine density and electrophysiological parameters, our transcriptome analysis highlighted Npas4 as a

regulator of genes that belong to the ontology group "regulation of locomotion" (Fig 4B). This led us to hypothesize that Npas4, through its observed effects on MSN function (spine density changes and electrophysiological parameters), might play a central role in regulating the locomotor response to cocaine. To test this hypothesis, we used shRNA-mediated knockdown of Npas4 in the nucleus accumbens with the same AAV-co-injection D1-labelling protocol as in Fig 5 (i.e. AAV-shscrambled or AAV-shNpas4 plus AAV-Flex-tdTomato and AAV-PPTA-Cre) and measured its impact on the locomotion of mice treated repeatedly with saline or cocaine (Fig 7A). In the habituation phase and in the chronic saline condition, Npas4 knockdown did not alter basal locomotion (Fig 7B). However, in line with our hypothesis of Npas4 as a determining factor of cocaine-induced hyperlocomotion, we observed a significant attenuation of the locomotor response by 20–40% from day 1 to 2 and on day 4 in the Npas4 knockdown animals (Fig 7B).

## Discussion

### Npas4 has a differential regulation pattern

The first central finding of our study is the differential regulation pattern of Npas4 in MSNs. Npas4 is sparsely expressed under
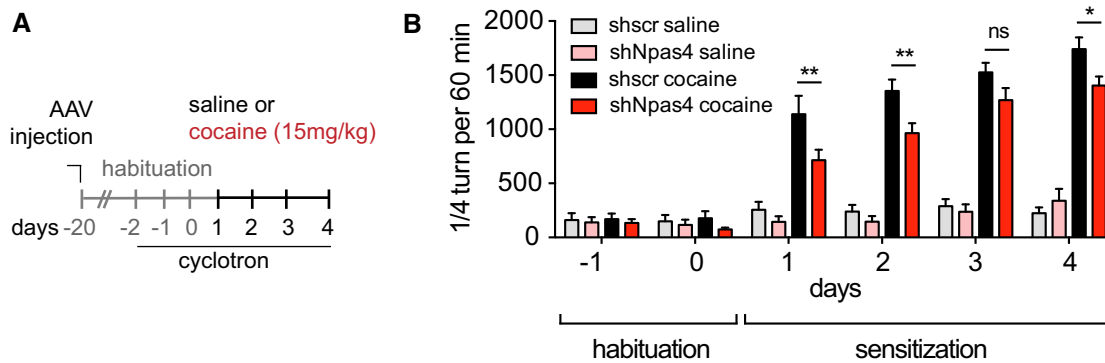
**Figure 7.  Npas4 gates cocaine-induced hyperlocomotion.**

A  Time course of AAV injections, habituation and treatments to assess the impact of Npas4 knockdown on cocaine-induced hyperlocomotion.

B  Cocaine-induced hyperlocomotion is attenuated by Npas4 knockdown while locomotor behaviour after saline injection is unaffected on all days. Mean + SEM; two-way ANOVA followed by Bonferroni *post-hoc* test. *$P < 0.05$, **$P < 0.01$, ns = not significant. $n = 12–16$ animals per condition.

control conditions (saline injections) and upregulated by cocaine *in vivo*. Our *in vitro* analysis indicated that it is preferentially induced by membrane depolarization (HiK) as compared to the D1-agonist SKF-38393, despite the last sharply inducing other IEGs, such as Arc. Npas4 induction is hence tightly coupled to membrane depolarization, which might enable the cell to discriminate different circuit inputs—and by extension probably even environmental signals—at the genome level and to drive downstream adaptations accordingly. Because we observed reduced dendritic spine density and altered electrophysiological parameters in the Npas4 knockdown group already before the first cocaine injection, and because the reaction to this first cocaine injection was attenuated, we infer that either baseline, non-cocaine-context related glutamatergic input onto MSNs in the home cage sustains Npas4 expression levels and mediates its subsequent cellular and behavioural effects or that saline injections and the novel context during habituation induce Npas4. Extending the differentiation at the synaptic level, Npas4 induction depends on different synapse-to-nucleus cascades than other IEGs tested in this study. Although all IEGs analysed here rely on NMDA receptor and VDCC signalling after membrane depolarization, only Fosb and Arc depend on PKA and MAPK signalling. Npas4 induction is independent of these cascades and in turn is partly regulated by calcineurin. The independence of Npas4 from PKA and MAPKs is highly interesting because these pathways are a crucial focus in addiction research and major targets for therapeutic concepts (Lee & Messing, 2008; Sun *et al*, 2016). Since these strategies would not interfere with Npas4 induction, our findings indicate that additional targets in the prevention and treatment of drug-related behaviour should be investigated, such as upstream regulators of Npas4 (i.e. calcineurin and nuclear calcium signalling) and Npas4 itself. We found that the ability of stimuli to upregulate Npas4 correlates with their ability to induce nuclear calcium transients (i.e. glutamate application and potassium chloride depolarization are able to induce nuclear calcium, but dopamine and SKF-38393 are not) and that induction of Npas4 is blocked by nuclear calcium antagonists. Further studies should investigate whether nuclear calcium signalling is relevant to drug-related behaviour. Our study reveals the signalling cascade of NMDARs/VDCCs-nuclear

$Ca^{2+}$-CaN/CaMK to be an essential regulator of Npas4 induction in MSNs. This pathway tightly controls Npas4 levels and subsequent neuronal remodelling and behaviour.

### Npas4 is a master regulator of neuronal transcription, regulating genes for synaptic proteins and calcium channels

Our gene ontology analysis of transcripts with altered levels upon Npas4 overexpression showed that Npas4 affects many cellular mechanisms, with a distinct focus on neuronal physiology (i.e. regulation of synapse assembly, regulation of learning and memory, regulation of neuron projection development). One caveat with our approach is that hippocampal neurons were used for this initial transcriptome analysis and that some genes in the overall transcriptome might differ in MSNs. qPCR analysis after overexpression and knockdown in MSNs shows that Npas4 regulates transcript levels of NMDA receptor subunits (Grin1, Grin2a and Grin2b), voltage-dependent calcium channel subunits (Cacna1c and Cacna1d) and the synaptic scaffolding protein Nptx2, most of these in an activity-dependent manner. At the transcriptional level, Npas4 is thus implicated in control over the magnitude of membrane ion signalling and synaptic transmission. Many of the synaptic genes we analysed are adjusted in the same direction in the development of addiction as they are in our study after Npas4 overexpression: upregulation of Nptx2 (Pacchioni *et al*, 2009), upregulation of Grin1 and Grin2b (Zhang *et al*, 2006; Schumann & Yaka, 2009), upregulation of Cacna1c (Renthal *et al*, 2009) and Cacna1d (Bernardi *et al*, 2014), suggesting that Npas4 might mediate at least some of these changes.

It is noteworthy that Npas4 regulates transcription of the genes for NMDAR subunits Grin1, Grin2a and Grin2b in MSNs, as NAc NMDA receptor activity has been shown to be required for expression of hyperlocomotion upon exposure to cocaine, heroin and intra-NAc dopamine infusions (Pulvirenti *et al*, 1991). This gives our results further relevance and possibly explains the phenotype of reduced cocaine-induced hyperlocomotion. Due to its potent transcriptional response, we hypothesize that the distinctive regulation pattern of Npas4 in MSNs has evolved to restrict its function to very

defined or powerful circuits inputs, possibly relating especially meaningful environmental signals to Npas4 output.

### Npas4 regulates spine density and MSN electrophysiology *in vivo*

Building on our finding that Npas4 regulates genes involved in synaptic structure and function, we focused our analysis of MSN network behaviour on dendritic spines (structure) and electrophysiological parameters (function). Our findings that Npas4 regulates dendritic spine density under basal conditions and contributes to cocaine-induced increased spine density in D1-MSNs, imply that it controls certain stimulus-independent and -dependent synaptic inputs onto MSNs. MSN spine density alterations are a prime example of drug-induced cellular changes (Dobi *et al*, 2011). We previously showed cocaine-induced increase of spine density in MSNs is associated with the formation new glutamatergic synapses impinging onto MSNs, especially D1R-MSNs (Heck *et al*, 2015; Dos Santos *et al*, 2017). Our study reveals Npas4 as a key molecular regulator of this synaptogenesis process.

To understand how Npas4 can already affect behaviour on the first day of cocaine administration, we analysed MSN electrophysiological parameters in naive animals in D1-positive, D1-negative and pooled MSNs. Npas4 controls MSN membrane excitability (as inferred from an increased rheobase and a decreased input/output gain function in the Npas4-knockdown animals) and firing rate. The rheobase and firing rate effect was only present in D1-negative MSNs, while the decrease in I/O gain function was seen in both D1-positive and D1-negative MSNs with however only the pooled cell group showing statistically significant differences. Npas4 also negatively regulates cortico-striatal transmission, as seen by a decreased paired-pulse facilitation in the Npas4-knockdown animals, with a more pronounced effect in D1-negative MSNs. In this electrophysiological dataset some of the effects seem to be dominant in D1-negative MSNs (especially rheobase and PPF), while others (I/O gain) occur in both D1-positive and D1-negative MSNs with similar magnitude. None of the effects are significant in D1-positive MSNs, which might either indicate an absence of a biological effect or it might be due to lower sample sizes in this dataset. The observation that some effects are stronger in D1-negative MSNs stands in an interesting contrast to our findings on dendritic spines, where the Npas4-knockdown effect was restricted to D1-positive MSNs. It could be that Npas4 regulates certain cellular parameters in different ways in different MSN subtypes and that adaptations in D1-negative MSNs are either synergistic or homeostatic (e.g. D1-negative MSNs change their activity in response to synaptic alterations in D1-positive MSNs to maintain circuit balance). The reduction in neuronal excitability after Npas4 knockdown together with an increased firing rate could enhance the coincidence detection properties of MSNs. The fact that Npas4 levels positively correlate with excitability in MSNs (which are GABAergic) complements a previous study which found that Npas4 regulates excitatory input onto GABAergic neurons (SST neurons in that case) (Spiegel *et al*, 2014). Decreasing Npas4 levels, as performed in our study, is hypothesized to decrease spontaneous depolarization (because of lower excitability) and increase cortical control over MSN activity and thus restrain hyperlocomotion upon cocaine exposure, possibly explaining the phenotype of reduced hyperlocomotion in the Npas4-knockdown group

in our study. Extrapolating to human phenotypes, sensitivity to drug effects and propensity to drug use might be an intrinsic fault in brain circuit programming where heightened Npas4 function leads to increased excitability and decreased cortical control of MSNs and an increase in drug-related behaviour.

### Npas4 regulates hyperlocomotion in response to cocaine and is a potential treatment target in human addiction

We found that although locomotor activity is unaffected in the Npas4-knockdown group after saline injections, animals with NAc Npas4-knockdown display attenuated hyperlocomotion in response to cocaine at the first injection. This phenomenon persists throughout the sensitization process so that animals in the knockdown group consistently show decreased cocaine hyperlocomotion. These results imply Npas4 as an important and specific determining factor of drug-induced hyperlocomotion that does not alter basal locomotor behaviour.

As Npas4 determines an animal's drug-dependent hyperlocomotion, Npas4 levels or the transcriptional output of its targets could potentially be used as markers in molecular screening concepts for addiction in humans. We hypothesize that manipulating Npas4 levels either directly (e.g. through CRISPR-Cas9-associated genome editing or direct Npas4-targeting vectors) or indirectly (e.g. through boosting/reducing nuclear calcium signalling) could be explored as a therapeutic strategy. What is especially intriguing about Npas4 as a treatment target is that changing Npas4 levels leaves basal locomotor behaviour unchanged, as shown in our study. This potential benefit of a more selective and context-dependent Npas4 action mechanism is also implied by a recent study, which showed that striatal Npas4 knockdown selectively decreased the rewarding properties of cocaine, but not of sucrose, while leaving aversion-learning intact (Taniguchi *et al*, 2017). Thus, Npas4 could perhaps be used as a highly specific and potent target of drug-specific therapeutic interventions. Since Npas4 levels are altered by environmental enrichment (Bloodgood *et al*, 2013), it is also feasible that behavioural therapeutic and preventative measures, such as environmental change and rehabilitation efforts, could be leveraged to alter Npas4 levels, change MSN structure and function as well as diminish propensity to drug use.

### Npas4 exerts its effects before the first cocaine injection

An interesting point in our results is that Npas4 influences MSN physiology already before cocaine is administered for the first time and it influences the reaction to the first cocaine injection. Npas4 knockdown decreased spine density, I/O gain and paired-pulse ratios as well as increased rheobase and firing rates in nucleus accumbens MSNs before the animals were ever exposed to cocaine. This implies that basal, non-drug-related neuronal activity already determines Npas4 function. Npas4 levels, possibly sustained by spontaneous depolarization, may determine the input properties of MSNs and hence perform a gating function that controls certain behavioural responses, such as hyperlocomotion, to drugs of abuse in the future. This is reminiscent of the functions of nuclear calcium-VEGFD signalling as recently discovered by our lab, wherein basal nuclear calcium and its downstream target VEGFD, independent of strong specific stimuli, determine dendritic

architecture and electrophysiological behaviour in hippocampal neurons *in vivo* and render neurons permissive for the formation of new memories (Hemstedt *et al*, 2017). Most studies on the functions of activity-induced genes such as Npas4 or cFos relate the activity-dependent increase in transcript levels to a specific, strong and short stimulus (i.e. electroshocks in fear memory paradigms, drug administration in addiction studies). It is then hypothesized that these IEGs, through their cellular effects within the next hours, consolidate the memory of this specific context in long-term changes in neuronal physiology. Yet, it might be that ongoing basal neural activity, not related to a particular context, is equally important for IEGs such as Npas4 to exert their function and shape behaviour. In line with this argument are observations that increased mental stimulation from an enriched environment can be protective against context-specific maladaptation such as addiction and anxiety (Solinas *et al*, 2008). Our study uncovers a new dimension to Npas4 function, where in addition to its reported roles in encoding context-specific memories, it controls essential aspects of neuronal physiology such as spine density and electrophysiological parameters independent of strong environmental signals. These changes, in turn, have profound influences on how an animal will react to future environmental stimuli.

### Conclusions and future directions

Our results establish Npas4 as a critical regulator of medium spiny neuron function and structure. This impact on striatal network activity translates to an essential gating function on locomotor activity after cocaine administration, while leaving basal locomotor behaviour unchanged. Our findings reveal that these potent effects of Npas4 are under the control of a signalling cascade in MSNs that does not involve molecular targets that have been of interest in drug-related behaviour in the past (i.e. MAPK and PKA pathways as upstream targets, and Fosb and Arc as transcriptional targets). The two central Npas4 properties of an induction that is independent of ubiquitous signalling cascades and a selective effect on cocaine-dependent hyperlocomotion suggest that it should be explored as a novel target in therapies for human drug-related behaviours. What makes our findings especially interesting in this regard is the fact that the differential nature of Npas4 induction is conserved in human iPSC-derived forebrain organoids, thereby opening the possibility that the above cascade might be targeted in the clinical treatment of addiction in humans.

# Materials and Methods

### Mouse neuron cultures

Striatal and hippocampal neuron cultures were prepared from neonatal C57BL/6N mice and cultured as previously described (Bading & Greenberg, 1991), with the following modifications. Dishes and coverslips were coated with Poly-L-Ornithine (100 mg/ml) for striatal neurons and with Poly-D-Lysine (2 mg/ml) and Laminin (10 μg/ml) for hippocampal neurons. 48 h prior to final experiments, the medium was changed from NBA to transfection medium. Cultures were maintained for 11–12 days, depending on the experiment (see Results section).

### Cell culture stimulation and pharmacological substances

For membrane depolarization (HiK), 0.41 volumes of an isosmotic solution were added to the medium as previously described (Hardingham *et al*, 1997) so that the final $K^+$ concentration was raised to 55 mM. For pathway stimulations we used glutamate (1 μM, Tocris), the D1-agonist SKF-38393 (10 μM, Tocris), dopamine (20 μM, BD Biosciences) and forskolin (10 μM, Sigma). Receptors, channels and pathways were blocked with SCH-23390 (10 μM, Tocris), TTX ($Na^+$ channels, 1μM, Biotrend), verapamil (L-type $Ca^{2+}$ channels, 30 μM, HelloBio), D/L-APV (NMDA receptors, 100 μM, Biotrend), UO126 (ERK1/2, 10 μM, Axxora), SB203580 (p38alpha, 10 μM, Calbiochem), SB202190 (p38beta, 10 μM, Tocris), Cyclosporin A (calcineurin,1 μM, Fluka), FK506 (calcineurin, 1 μM, Axxora), H-89 (PKA, 10 μM, Sigma).

### Forebrain organoids

Organoids with a forebrain phenotype were generated from human induced pluripotent stem cells (hiPSCs) as previously described (Pasca *et al*, 2015) with modifications. A human D1 iPSC line was obtained from Dr. Jochen Utikal (DKFZ, Germany). It was generated from healthy human fibroblasts with an inducible polycistronic lentiviral reprogramming vector encoding for KLF4, MYC, POU5F1 and SOX2 (Horschitz *et al*, 2015). Approximately $10^4$ hiPSCs were aggregated and transferred into low attachment plates. For neuronal induction, dual SMAD inhibition (Chambers *et al*, 2009) was performed by addition of recombinant Noggin (100 ng/ml, R&D Systems), Dorsomorphin (500 nM, Tocris) and SB 431542 (10 μM, Tocris) to the culture medium for the first 7 days. On day 2, FGF2 (10 ng/ml, Peprotech) was added. From day 7 to 21, free-floating organoids were maintained in neural medium (Neurobasal, B27 without Vitamin A, Glutamax; all Thermo Fisher) supplemented with FGF2 (10 ng/ml) and EGF (10 ng/ml). On day 22, FGF2 and EGF were replaced by BDNF (10 ng/ml, Peprotech) and NT-3 (10 ng/ml, Peprotech) to support differentiation. From day 35 onwards, organoids were kept in neural medium without growth factors. Wnt and Sonic hedgehog pathway inhibitors (IWP-2, 2 μM, Sigma and Cyclopamine, 1 μM, Merck) were included in the culture media from day 0 to day 35 to ensure forebrain fate adoption.

### Quantitative real-time PCR

Total RNA was isolated using the RNeasy MiniKit (Qiagen). 0.5–1 μg of RNA was reverse transcribed to cDNA using random primers and the High Capacity cDNA Reverse Transcription Kit (Thermo Fisher Scientific). For all qPCR experiments except those in forebrain organoids in Fig 2F and G, the TaqMan platform (Applied Biosystems) was used. For qPCR experiments in forebrain organoids, a custom SYBR green (Applied Biosystems) assay was used. Relative quantification for TaqMan analysis was performed with the ΔΔCt method using TaqMan probes, qPCR Master Mix (Life Technologies) and an ABI7300 thermal cycler (Thermo Fisher). Gusb was used as the endogenous reference gene and all samples were run as duplicates. The following TaqMan probes (Thermo Fisher Scientific) were used: gusb (Mm00446953_m1), npas4 (Mm00463644_m1), fosb (Mm00500401_m1), arc (Mm00479619_g1), egr1 (Mm00656724_m1), inhba (Mm00434338_m1), cfos (Mm00487425_m1), grin1 (Mm00433790_m),

grin2a (Mm00433802_m1), grin2b (Mm00433820_m1), nptx2 (Mm00479438_m1), cacna1c (Mm01188822_m1), cacna1d (Mm01209919_m1), gria1 (Mm00433753_m1), gria3 (Mm00497506_m1). The cycling conditions were as follows: (1×) 2 min at 50°C, (1×) 10 min at 95°C, (55×) 15 s at 95°C and 1 min at 60°C, (1×) until sample collection at 4°C. For SYBR green assays, TBP was used as an endogenous reference gene. The following primers were used: Npas4 (Sense: GTGAGGCTACAGGCCAAGAC

Antisense: AGGGCAGCATGGTCGGAGTG)

Arc (Sense: AAGTCGCACACGCAGCAGAGCA, Antisense: AGGCGGGCGTGAATCACTGGA), TBP (Sense: GCCTTGTGCTCACCCAC-CAACAATTT, Antisense: GGTACATGAGAGCCATTACGTC). PCR conditions were as follows: Denaturing: 10 min at 95°C, Cycling (30×): 10 s at 95°C, 10 s at 60°C, 15 s at 72°C.

## type="main">Ca$^{2+}$-imaging protocol

Ca$^{2+}$-imaging was performed as previously described (Mauceri *et al*, 2015), with modifications. Neurons were kept in SGG minimal medium at all times during imaging ("salt-glucose-glycine", 140.1 mM NaCl, 5.3 mm KCl, 1 mM MgCl$_2$, 2 mM CaCl$_2$, 10 mM HEPES, 30 mM glucose, 1 mm glycine, 0.5 mM sodium pyruvate). For experiments with GCaMP3-NLS, coverslips with infected neurons were taken out of the incubator, equilibrated in SGG for 10 min and positioned under the microscope in 1ml SGG to commence imaging. Stimulations were performed by washing out the baseline SGG solution and washing in a solution with SGG and the pharmacological of interest.

## type="main">Ca$^{2+}$-imaging analysis

For GCaMP3-NLS imaging, fluorescence traces were plotted as $\Delta F/F_0 = (F - F_0)/F_0$, with $F$ representing the background-subtracted fluorescence intensity at the given time point and $F_0$ representing the average fluorescence intensity from a baseline time interval at the beginning of the trial.

## Recombinant adeno-associated viruses and stereotaxic injections

AAVs with serotype 1/2 were prepared by heparin column purification as previously described (Zhang *et al*, 2007). Neuronal cultures were infected with the constructs indicated in the results section at DIV5. For *in vivo* studies, D1R-MSN and D2R-MSN were labelled by expressing Cre recombinase under the promoter of PPTA (preprotachykinin) and ENK (preproenkephalin), respectively. Serotype 9 AAV-PPTA-Cre and AAV-ENK-Cre were generated by Dr. A. Bemelmans (CEA, Molecular Imaging Center (MIRCen); CNRS/UMR9199). The co-injection with the AAVrh9-pCAG-flex-tdTomato-WRPE (AddGene) allowed the Cre-dependent expression of tdTomato under the CMV/actin hybrid promoter (CAG). For morphological analysis of single dendrites, AAV shNpas4-GFP or AAV shscr-GFP were co-injected with a mix of either PPTA-Cre or ENK-Cre and flex-tdTomato in a 1/10,000 ratio, which allows the sparse labelling of either D1R-MSNs or D2-MSNs (Dos Santos *et al*, 2017). For electrophysiological recordings, AAVs expressing shNpas4-GFP or shscr-GFP were co-injected with a mix of either PPTA-Cre or ENK-Cre and flex-tdTomato in a ratio of 1/1,000 to densely label either D1R-MSNs or D2-MSNs. Mice were injected at 7 weeks of age at the

following stereotaxic coordinates: +1.7 mm rostral to the bregma, 1.2 mm lateral to midline and 4.6 mm ventral to the skull surface. The rate of injection was 0.15 μl/min with a total volume of 1 μl per striatum. Experiments were carried out after an incubation period of 3 weeks.

## Immunocytochemistry

For immunocytochemistry, neurons on glass coverslips were fixed in PBS containing 4% paraformaldehyde and 4% sucrose for 10 min, permeabilized with 0.3% Triton X-100 for 10 min and blocked in 10% normalized goat serum for 1 h. Subsequently, samples were incubated with primary antibody in solution (PBS, 1% NGS and 0.1% Triton X-100) overnight and washed five times with PBS. Antibodies were used as follows: Darpp-32 (1:1,000, rabbit, Cell Signaling, mAb 2306), Map-2 (1:1,000, mouse, Millipore, MAB3418), GFP (1:1,000, Molecular Probes, A11120). Next, cells were incubated with the same solution but secondary antibodies instead and washed five times in PBS followed by staining with Hoechst (1:3,000). Coverslips were then mounted on glass microscope slides with Mowiol.

## Microarray experiments and transcriptome analysis

Hippocampal neurons were infected with rAAV-Npas4-flag of rAAV-GFP-myc for overexpression at DIV5 and harvested at DIV11. For microarray transcriptome analysis we used Illumina MouseWG-6 v2.0 Expression BeadChips®. RNA samples were processed by the Genomics and Proteomics Core Facility at the DKFZ, Heidelberg. Three biological replicates were performed per condition. RNA quality was assessed using the Nanodrop ND-1000 (Agilent 2100 Bioanalyzer). A total of 4 μg of the RNA was used for each microarray replicate. Raw microarray data was analysed (DKFZ, Germany) using Chipster (Kallio *et al*, 2011) with R and Bioconductor packages. Statistical tests are *t*-tests over all beads (e.g. for one probeID over all beads of all samples of a group) in original scale. Benjamini-Hochberg correction is applied over all *P*-values of the differential expression analysis. A false discovery rate (FDR) of 5% was utilized as a cut-off for determination of significance. The official gene symbols for the genes enriched in the up- or downregulated groups (1.5-fold cut-off in either direction) were fed into the PANTHER online tool (http://www.pantherdb.org/; analysis type: PANTHER overrepresentation test, release: 20170413; GO Ontology database released 2017-05-25) (Mi *et al*, 2013). Analysis settings were for biological process and statistical overrepresentation.

## Animals and treatments

Six-week-old male C57BL/6 mice were purchased from Janvier (Le Genest, St. Isle, France) and maintained in a 12 h light/dark cycle in stable conditions of temperature (21 ± 1°C) and humidity (60%) with *ad libidum* access to food and water. Animals were habituated to the animal facility for 1 week prior to the experiments. Animal care was conducted in accordance with standard ethical guidelines (NIH publication no. 85-23, revised 1985 and European Community Guidelines on the Care and Use of Laboratory Animals [86/609/EEC]). The experiments were approved by the local ethics committee "Comité d'Ethique en Experimentation Animale Charles Darwin

C2EA-05". Cocaine hydrochloride (Sigma-Aldrich, St. Louis, MO) was dissolved in a 0.9% NaCl (w/v) aqueous solution (saline) and administrated intraperitoneally at 15 mg/kg in a volume of 10 ml/kg.

## Cocaine administration, tissue preparation and immunohistochemistry

After 3 days of daily handling and habituation to an injection of saline solution, mice received a daily injection of saline or cocaine (15 mg/kg) for 5 days in their home cage. At the indicated time after the last saline or cocaine injection (see legends in Figs 1, 5, and 7), mice were rapidly anaesthetized with an intraperitoneal injection of pentobarbital (50 mg/kg; Sanofi-Aventis, Paris, France) and perfused transcardially with a fixative solution containing 4% paraformaldehyde (PFA) (w/v) in 0.1 M $Na_2HPO_4/Na_2HPO_4$, pH 7.5 at 4°C delivered with a peristaltic pump at 20 ml/min for 5 min. The brain was removed from the skull, post-fixed overnight in 4% PFA, and stored at 4°C. Sections of 30 μm thickness were cut in the frontal plane with a vibratome (Leica, Nussloch, Germany) and kept at −20°C in a solution containing 30% ethylene glycol (v/v), 30% glycerol (v/v) and 0.1 M phosphate buffer. Sections were then processed for immunohistochemistry as follows. Free-floating sections were rinsed three times for 10 min in Tris-buffered saline (TBS; 25 mM Tris–HCl and 0.5 M NaCl, pH 7.5) followed by a blocking and permeabilization step of 1 h at RT in 5% normal goat serum and 0.1% Triton X-100 (Sigma-Aldrich) in TBS. After three rinses in TBS, the sections were incubated overnight at 4°C with a rabbit anti-Npas4 antibody (gift from Dr. Micheal E. Greenberg, Harvard) diluted at 1:500 and a mouse anti-NeuN antibody (Merck-Millipore) diluted at 1:1,000 or a rabbit anti-Fos antibody (Santa Cruz; sc-166940) diluted 1:500 in blocking buffer described above. Sections were rinsed three times for 10 min in TBS and incubated for 90 min at RT in TBS with a goat anti-rabbit Cy3-conjugated secondary antibody (1:500) and/or a goat anti-mouse Alexa 488 secondary antibody (1:500) from Invitrogen. After three rinses in TBS, sections were incubated for 5 min with Hoechst (Invitrogen) to counterstain the nuclei. Sections were rinsed three times for 10 min in TBS and three times for 10 min in Tris Buffer (0.25 M Tris) before mounting in Vectashield (Vector Laboratories). Quantifications of Npas4- and Fos-positive cells are represented as fold increase normalized to the saline group. The fold increase represents the ratio of the number of Npas4-positive cells in the cocaine-treated group over the number of Npas4-positive cells in the saline group. Quantifications were performed from $n = 4$ mice per group. One slice per mouse was used, which corresponds to 0.98 mm from the Bregma since it offers the ability to analyse the NAc core and shell subdivisions and the dorsal striatum from a single brain slice. For each mouse, 10 images were acquired for the NAc (five images per hemisphere) and 10 images for the dorsal striatum (five per hemisphere). Statistical analyses were performed using the number of mice as the $n$.

## Spine density analysis

Image stacks were taken using a confocal laser scanning microscope (SP5, Leica) equipped with a 1.4 NA objective. The pinhole aperture was set to 1 Airy unit, pixel size to 60 nm and z-step to 210 nm. The excitation wavelength was 488 nm for GFP and 561 nm for tdTomato, with emission ranges of 500–550 and 570–650 nm, respectively. Deconvolution with experimental point spread function from fluorescent beads using a maximum likelihood estimation algorithm was performed with Huygens software (Scientific Volume Imaging). Neuronstudio software was used to reconstruct the dendrite and detect dendritic spines with manual correction. Segments of secondary dendrites of at least 40 microns in length were analysed.

## Statistical analysis of spine imaging and locomotor data

Data are displayed as mean ± SEM, and statistical analysis was performed with GraphPad Prism software (University of Southampton, Southampton, UK). Where appropriate, unpaired Student's *t*-test or two-way ANOVA (repeated-measure in the case of locomotor sensitization) followed by the *post-hoc* Bonferroni comparisons were performed.

## Brain slice preparation and patch-clamp recordings

All experiments were performed in accordance with the guidelines of the local animal welfare committee (Center for Interdisciplinary Research in Biology Ethics Committee) and the EU (directive 2010/63/EU). Every precaution was taken to minimize stress and the number of animals used in each series of experiments. Animals were housed in standard 12-h light/dark cycles, and food and water were available *ad libitum*. For brain slices preparation, oblique parasagittal (10°) brain slices containing the prefrontal cortex and the corresponding corticostriatal projection field in the nucleus accumbens were prepared from mice (P60-P80) using a vibrating blade microtome (VT1200S, Leica Micosystems, Nussloch, Germany). Brains were sliced in a 5% $CO_2$/95% $O_2$-bubbled, ice-cold cutting solution containing in mM: 125 NaCl, 2.5 KCl, 25 glucose, 25 $NaHCO_3$, 1.25 $NaH_2PO_4$, 2 $CaCl_2$, 1 $MgCl_2$, 1 pyruvic acid, and then transferred into the same solution at 34°C for 1 h and then moved to room temperature. For patch-clamp recordings, borosilicate glass pipettes of 4–6 MΩ resistance contained for whole-cell recordings (in mM): 105 K-gluconate, 30 KCl, 10 HEPES, 10 phosphocreatine, 4 ATP-Mg, 0.3 GTP-Na, 0.3 EGTA (adjusted to pH 7.35 with KOH). The composition of the extracellular solution was (mM): 125 NaCl, 2.5 KCl, 25 glucose, 25 $NaHCO_3$, 1.25 $NaH_2PO_4$, 2 $CaCl_2$, 1 $MgCl_2$, 10 μM pyruvic acid bubbled with 95% $O_2$ and 5% $CO_2$. Signals were amplified using EPC10-2 amplifiers (HEKA Elektronik, Lambrecht, Germany). All recordings were performed at 34°C using a temperature control system (Bath-controller V, Luigs&Neumann, Ratingen, Germany) and slices were continuously superfused at 2–3 ml/min with the extracellular solution. Slices were visualized on an Olympus BX51WI microscope (Olympus, Rungis, France) using a 4×/0.13 objective for the placement of the stimulating electrode and a 40×/0.80 water-immersion objective for localizing cells for whole-cell recordings. The series resistance was not compensated. Recordings were sampled at 10 kHz, using the Patchmaster v2x32 program (HEKA Elektronik). Paired-pulses protocols. Electrical stimulations were performed with a bipolar electrode (Phymep, Paris, France) placed in the infralimbic cortex (layer V). Electrical stimulations were monophasic at constant current (ISO-Flex

stimulator, AMPI, Jerusalem, Israel). Currents were adjusted to evoke 50-200pA EPSCs. 20 successive EPSCs were individually measured and then averaged. Variation of input and series resistances above 20% led to the rejection of the experiment.

**Electrophysiological data analysis**

Off-line analysis was performed with Fitmaster (Heka Elektronik) and Matlab R2016a (Mathworks). Passive and active membrane properties were obtained from 10 pA depolarizing current steps of 500 ms duration from −70 mV holding membrane potential. Input resistance and membrane time constant were measured from voltage traces obtained at −50 pA hyperpolarizing current step. Membrane time constant was estimated from a double exponential fit to the negative deflection of membrane voltage. Sag ratio was calculated for steps in which the voltage deflection reached values between −110 and −90 mV, as the ratio of the maximal negative potential, from 0 to 150 ms, divided by the mean steady state voltage deflection. AP half width duration was measured from the half-height of the AP rising phase. Rise and decay times were calculated from 10 to 90% of the AP waveform. Firing rate was calculated at 2-fold rheobase current step. The input/output gain function was measured as the slope of the linear fit of f-I curve from the rheobase. Statistical analysis was performed with Prism 5.02 software (San Diego, CA, USA). All results are expressed as mean ± SEM. Statistical significance was assessed in non-parametric Mann–Whitney, one-sample *t*-tests and Kruskal-Wallis test using the indicated significance threshold (*P*).

**Locomotor sensitization**

Locomotor activity was measured in a circular corridor (i.e. cyclotron) containing four infrared beams placed at every 90° (Immetronic, Pessac, France). Locomotor activity was expressed as a cumulative count of crossings between quarters of the cyclotron during 60 min. The locomotor sensitization protocol consisted in four daily sessions during which mice are placed in the activity boxes for 30 min prior and 60 min after an injection of saline or cocaine solution. To assess the efficacy of shNpas4, mice received a fifth injection of a saline or cocaine solution and were perfused (see Tissue preparation section) 1 h after the injection of saline or cocaine to perform Npas4 immunohistological staining and dendritic spine analysis.

**Statistical analysis**

Statistical analysis was performed in Excel (Microsoft) or Prism (GraphPad). ANOVA *P*-values and *F*-stats can be found in Table EV2.

# Data availability

The Npas4 overexpression gene expression microarray raw data from Fig 4 is available at Array Express with accession E-MTAB-10706 (link: https://www.ebi.ac.uk/arrayexpress/experiments/E-MTAB-10706/).

**Expanded View** for this article is available online.

# References

Bading H, Greenberg ME (1991) Stimulation of protein tyrosine phosphorylation by NMDA receptor activation. *Science* 253: 912–914

Bernardi RE, Uhrig S, Spanagel R, Hansson AC (2014) Transcriptional regulation of L-type calcium channel subtypes Cav1.2 and Cav1.3 by nicotine and their potential role in nicotine sensitization. *Nicotine Tob Res* 16: 774–785

Bloodgood BL, Sharma N, Browne HA, Trepman AZ, Greenberg ME (2013) The activity-dependent transcription factor NPAS4 regulates domain-specific inhibition. *Nature* 503: 121–125

Britt JP, Benaliouad F, McDevitt RA, Stuber GD, Wise RA, Bonci A (2012) Synaptic and behavioral profile of multiple glutamatergic inputs to the nucleus accumbens. *Neuron* 76: 790–803

Brown TE, Lee BR, Mu P, Ferguson D, Dietz D, Ohnishi YN, Lin Y, Suska A, Ishikawa M, Huang YH *et al* (2011) A silent synapse-based mechanism for cocaine-induced locomotor sensitization. *J Neurosci* 31: 8163–8174

Chambers SM, Fasano CA, Papapetrou EP, Tomishima M, Sadelain M, Studer L (2009) Highly efficient neural conversion of human ES and iPS cells by dual inhibition of SMAD signaling. *Nat Biotechnol* 27: 275–280

Dobi A, Seabold GK, Christensen CH, Bock R, Alvarez VA (2011) Cocaine-induced plasticity in the nucleus accumbens is cell specific and develops without prolonged withdrawal. *J Neurosci* 31: 1895–1904

Dos Santos M, Salery M, Forget B, Garcia Perez MA, Betuing S, Boudier T, Vanhoutte P, Caboche J, Heck N (2017) Rapid synaptogenesis in the nucleus accumbens is induced by a single cocaine administration and stabilized by mitogen-activated protein kinase interacting kinase-1 activity. *Biol Psychiatry* 82: 806–818

Dos Santos M, Cahill EN, Bo GD, Vanhoutte P, Caboche J, Giros B, Heck N (2018) Cocaine increases dopaminergic connectivity in the nucleus accumbens. *Brain Struct Funct* 223: 913–923

Hardingham GE, Chawla S, Johnson CM, Bading H (1997) Distinct functions of nuclear and cytoplasmic calcium in the control of gene expression. *Nature* 385: 260–265

Heck N, Dos Santos M, Amairi B, Salery M, Besnard A, Herzog E, Boudier T, Vanhoutte P, Caboche J (2015) A new automated 3D detection of synaptic contacts reveals the formation of cortico-striatal synapses upon cocaine treatment *in vivo*. *Brain Struct Funct* 220: 2953–2966

Hemstedt TJ, Bengtson CP, Ramirez O, Oliveira AMM, Bading H (2017) Reciprocal interaction of dendrite geometry and nuclear calcium-VEGFD signaling gates memory consolidation and extinction. *J Neurosci* 37: 6946–6955

Hester I, McKee S, Pelletier P, Thompson C, Storbeck C, Mears A, Schulz JB, Hakim AA, Sabourin LA (2007) Transient expression of Nxf, a bHLH-PAS transactivator induced by neuronal preconditioning, confers neuroprotection in cultured cells. *Brain Res* 1135: 1–11

Hikida T, Kimura K, Wada N, Funabiki K, Nakanishi S (2010) Distinct roles of synaptic transmission in direct and indirect striatal pathways to reward and aversive behavior. *Neuron* 66: 896–907

Horschitz S, Matthäus F, Groß A, Rosner J, Galach M, Greffrath W, Treede RD, Utikal J, Schloss P, Meyer-Lindenberg A (2015) Impact of preconditioning with retinoic acid during early development on morphological and functional characteristics of human induced pluripotent stem cell-derived neurons. *Stem Cell Res (Amst)* 15: 30–41

Kallio MA, Tuimala JT, Hupponen T, Klemela P, Gentile M, Scheinin I, Koski M, Kaki J, Korpelainen EI (2011) Chipster: user-friendly analysis software for microarray and other high-throughput data. *BMC Genom* 12: 507

Kita K, Shiratani T, Takenouchi K, Fukuzako H, Takigawa M (1999) Effects of D1 and D2 dopamine receptor antagonists on cocaine-induced self-stimulation and locomotor activity in rats. *Eur Neuropsychopharmacol* 9: 1–7

Kravitz AV, Tye LD, Kreitzer AC (2012) Distinct roles for direct and indirect pathway striatal neurons in reinforcement. *Nat Neurosci* 15: 816–818

Lee AM, Messing RO (2008) Protein kinases and addiction. *Ann N Y Acad Sci* 1141: 22–57

Macias W, Carlson R, Rajadhyaksha A, Barczak A, Konradi C (2001) Potassium chloride depolarization mediates CREB phosphorylation in striatal neurons in an NMDA receptor-dependent manner. *Brain Res* 890: 222–232

Mauceri D, Hagenston AM, Schramm K, Weiss U, Bading H (2015) Nuclear calcium buffering capacity shapes neuronal architecture. *J Biol Chem* 290: 23039–23049

McGregor A, Roberts DC (1993) Dopaminergic antagonism within the nucleus accumbens or the amygdala produces differential effects on intravenous cocaine self-administration under fixed and progressive ratio schedules of reinforcement. *Brain Res* 624: 245–252

Mi H, Muruganujan A, Casagrande JT, Thomas PD (2013) Large-scale gene function analysis with the PANTHER classification system. *Nat Protoc* 8: 1551–1566

Pacchioni AM, Vallone J, Worley PF, Kalivas PW (2009) Neuronal pentraxins modulate cocaine-induced neuroadaptations. *J Pharmacol Exp Ther* 328: 183–192

Paşca AM, Sloan SA, Clarke LE, Tian Y, Makinson CD, Huber N, Kim CH, Park J-Y, O'Rourke NA, Nguyen KD *et al* (2015) Functional cortical neurons and astrocytes from human pluripotent stem cells in 3D culture. *Nat Methods* 12: 671–678

Pascoli V, Besnard A, Herve D, Pages C, Heck N, Girault JA, Caboche J, Vanhoutte P (2011a) Cyclic adenosine monophosphate-independent tyrosine phosphorylation of NR2B mediates cocaine-induced extracellular signal-regulated kinase activation. *Biol Psychiatry* 69: 218–227

Pascoli V, Turiault M, Luscher C (2011b) Reversal of cocaine-evoked synaptic potentiation resets drug-induced adaptive behaviour. *Nature* 481: 71–75

Pascoli V, Terrier J, Espallergues J, Valjent E, O'Connor EC, Luscher C (2014) Contrasting forms of cocaine-evoked plasticity control components of relapse. *Nature* 509: 459–464

Piazza PV, Deminiere JM, Le Moal M, Simon H (1989) Factors that predict individual vulnerability to amphetamine self-administration. *Science* 245: 1511–1513

Pierce RC, Kalivas PW (1997) A circuitry model of the expression of behavioral sensitization to amphetamine-like psychostimulants. *Brain Res Brain Res Rev* 25: 192–216

Pulvirenti L, Swerdlow NR, Koob GF (1991) Nucleus accumbens NMDA antagonist decreases locomotor activity produced by cocaine, heroin or accumbens dopamine, but not caffeine. *Pharmacol Biochem Behav* 40: 841–845

Renthal W, Kumar A, Xiao G, Wilkinson M, Covington HE, Maze I, Sikder D, Robison AJ, LaPlant Q, Dietz DM *et al* (2009) Genome-wide analysis of chromatin regulation by cocaine reveals a role for sirtuins. *Neuron* 62: 335–348

Schlumm F, Mauceri D, Freitag HE, Bading H (2013) Nuclear calcium signaling regulates nuclear export of a subset of class IIa histone deacetylases following synaptic activity. *J Biol Chem* 288: 8074–8084

Schumann J, Yaka R (2009) Prolonged withdrawal from repeated noncontingent cocaine exposure increases NMDA receptor expression and ERK activity in the nucleus accumbens. *J Neurosci* 29: 6955–6963

Solinas M, Chauvet C, Thiriet N, El Rawas R, Jaber M (2008) Reversal of cocaine addiction by environmental enrichment. *Proc Natl Acad Sci USA* 105: 17145–17150

Spiegel I, Mardinly AR, Gabel HW, Bazinet JE, Couch CH, Tzeng CP, Harmin DA, Greenberg ME (2014) Npas4 regulates excitatory-inhibitory balance within neural circuits through cell-type-specific gene programs. *Cell* 157: 1216–1229

Sun WL, Quizon PM, Zhu J (2016) Molecular mechanism: ERK signaling, drug addiction, and behavioral effects. *Prog Mol Biol Transl Sci* 137: 1–40

Sun X, Lin Y (2016) Npas4: linking neuronal activity to memory. *Trends Neurosci* 39: 264–275

Taniguchi M, Carreira MB, Cooper YA, Bobadilla A-C, Heinsbroek JA, Koike N, Larson EB, Balmuth EA, Hughes BW, Penrod RD *et al* (2017) HDAC5 and its target gene, Npas4, function in the nucleus accumbens to regulate cocaine-conditioned behaviors. *Neuron* 96: 130–144.e136

Zhang S-J, Steijaert MN, Lau D, Schutz G, Delucinge-Vivier C, Descombes P, Bading H (2007) Decoding NMDA receptor signaling: identification of genomic programs specifying neuronal survival and death. *Neuron* 53: 549–562

Zhang J, Zhang L, Jiao H, Zhang Q, Zhang D, Lou D, Katz JL, Xu M (2006) c-Fos facilitates the acquisition and extinction of cocaine-induced persistent changes. *J Neurosci* 26: 13287–13296

Zhang SJ, Zou M, Lu L, Lau D, Ditzel DA, Delucinge-Vivier C, Aso Y, Descombes P, Bading H (2009) Nuclear calcium signaling controls expression of a large gene pool: identification of a gene program for acquired neuroprotection induced by synaptic activity. *PLoS Genet* 5: e1000604